Monthly Notices
of the
ROYAL ASTRONOMICAL SOCIETY

MNRAS **449,** 3613–3619 (2015) doi:10.1093/mnras/stv507

# ExoMol molecular line lists – IX. The spectrum of AlO

Andrei T. Patrascu,* Sergei N. Yurchenko and Jonathan Tennyson

*Department of Physics and Astronomy, University College London, London WC1E 6BT, UK*

Accepted 2015 March 4. Received 2015 February 21; in original form 2014 December 12

## ABSTRACT

Accurate line lists are calculated for aluminium monoxide covering the pure rotation, rotation–vibration and electronic ($B - X$ blue–green and $A - X$ infrared bands) spectrum. Line lists are presented for the main isotopologue, $^{27}Al^{16}O$, as well as for $^{27}Al^{17}O$, $^{27}Al^{18}O$ and $^{26}Al^{16}O$. These line lists are suitable for high temperatures (up to 8000 K) including those relevant to exoplanetary atmospheres and cool stars. A combination of empirical and ab initio methods is used: the potential energy curves were previously determined to high accuracy by fitting to extensive data from analysis of laboratory spectra; a high-quality ab initio dipole moment curve is calculated using quadruple zeta basis set and the multireference configuration interaction method. Partition functions plus full line lists of transitions are made available in an electronic form as supplementary data to this paper and at www.exomol.com.

**Key words:** molecular data – opacity – astronomical data bases: miscellaneous – planets and satellites: atmospheres – stars: low-mass.

## 1 INTRODUCTION

Aluminium monoxide (AlO) is an interesting astronomical species whose spectrum is prominent in a new class of Nova-stars first discovered by Tenenbaum & Ziurys (2009) of which the most prominent examples are probably V838 Mon and V4332 Sgr (Merrill, Keenan & Deutsch 1962; Bernard & Gravina 1984; Banerjee et al. 2005, 2012; Tylenda et al. 2005). These two objects defined a new type of eruptive variables called intermediate-luminosity red transients and the observational data showed the intense presence of the near-infrared $A - X$ system of the AlO radical. Indeed this $A - X$ band is also found to be fairly prominent in a variety of cool, oxygen-rich stars (Bernard & Gravina 1984; Banerjee et al. 2012): besides the Mira variables discussed above AlO emissions were also observed in the OH/IR stars and two bright infrared sources (Banerjee et al. 2012).

Transitions in the blue–green $B - X$ system have been observed in sunspots (Sriramachandran, Viswanathan & Shanmugavel 2013) and the red supergiant VY Canis Majoris (Kaminski, Schmidt & Menten 2013), in which millimetre-wave rotational transitions have also been observed (Tenenbaum & Ziurys 2009). Finally, AlO spectra have been used to try and determine abundance of the long-lived, radioactive $^{26}Al$ isotope (Banerjee et al. 2004).

Terrestrially AlO emissions arise from rocket exhausts in the atmosphere (Johnson 1965; Knecht et al. 1996). Its spectrum is also extensively used in the laboratory to monitor AlO in plasmas and other applications (Bescos, Morley & Urena 1995; Naulin & Costes 1999; Glumac, Servaites & Krier 2001; Zhang & Li 2003; Bai et al. 2014; Surmick & Parigger 2014).

These applications, combined with technological uses of AlO spectra, have motivated a number of laboratory studies which have produced molecular constants characterizing the lowest three states of AlO $X^2\Sigma^+$, $A^2\Pi$ and $B^2\Sigma^+$. There have also been attempts to produce line lists. Parigger & Hornkohl (2011) constructed a comprehensive line list for the $X - B$ system for temperatures up to 6000 K but did not provide a transition dipole, so all their transition intensities are only relative. Launila & Berg (2011) performed a combined analysis of the $A - X$ and $B - X$ band systems involving 21 500 lines; we compare with some of their results below. There is, however, no single line list that combines a comprehensive set of transition frequencies with an accurate model for the transition intensities. It is this that we aim to do here as part of the ExoMol project. ExoMol aims to provide line lists of spectroscopic transitions for key molecular species which are likely to be important in the atmospheres of extrasolar planets and cool stars; its aims, scope and methodology have been summarized by Tennyson & Yurchenko (2012). Line lists for $^2\Sigma^+$ $X$H molecules, $X$ = Be, Mg, Ca, have already been published (Yadin et al. 2012), as well as for a number of closed-shell diatomics (Barton, Yurchenko & Tennyson 2013; Barton et al. 2014; Yorke et al. 2014). In this paper, we present rotation–vibration transition lists and associated spectra for AlO. These line lists are particulary comprehensive and should be valid for temperatures up to 8000 K.

## 2 METHOD

Rotation–vibration line lists for the three lower electronic states of AlO were obtained by direct solution of the nuclear motion

* E-mail: andrei.patrascu.11@ucl.ac.uk (ATP); s.yurchenko@ucl.ac.uk (SNY); j.tennyson@ucl.ac.uk (JT)

**Table 1.** Ab initio electric dipole and transition dipole moments in Debye at $R = 1.76$ Å.

| Transition moments | This Work | Zenouda et al. (1999)[a] |
|---|---|---|
| $X\,^2\Sigma^+$ | − 4.39 | − 4.24 |
| $A\,^2\Pi$ | − 1.30 | − 1.40 |
| $B\,^2\Sigma^+$ | − 2.18 | − 2.27 |
| $X\,^2\Sigma^+ - B\,^2\Sigma^+$ | 1.85 | 1.66 |
| $X\,^2\Sigma^+ - A\,^2\Pi$ | 0.61 | 0.61 |
| $B\,^2\Sigma^+ - A\,^2\Pi$ | − 0.046 | |

*Note.* [a]The signs of the diagonal dipoles have been changed to conform to the convention used by MOLPRO.

Schrödinger equation using program DUO (Yurchenko et al. 2015). The calculations require both a potential energy curve (PEC) for each of the three states considered and also couplings between these curves. These curves were taken from our previous study (Patrascu et al. 2014), which computed ab initio potential energies, spin–orbit and electronic angular momenta couplings, and refined them using available experimental data. Nuclear motion calculations using these refined curves showed that the observed transition frequencies and energy levels could be reproduced with root mean square error of only 0.07 $cm^{-1}$. In order to cover all vibrational excitations below 35 000 $cm^{-1}$, we have increased the sizes of the vibrational basis set to 90 for each of the $X$, $A$ and $B$ states from those used by Patrascu et al. (2014). The ranges of rotational excitations are listed in Table 2.

### 2.1 Dipole moments

There appears to be no experimental measurements of any AlO transition dipoles. For this reason we constructed new dipole moment curves (DMC) using high level ab initio calculations. These are compared to previous, high-level ab initio determinations (Zenouda et al. 1999) below. The ab initio calculations were performed using MOLPRO (Werner et al. 2010); we used multireference configuration interaction (MRCI) methods with different choices of basis sets. Our optimal basis choice was aug-cc-pVQZ; the active space used in MOLPRO representation was (9,4,4). Electronic dipole moments as function of bondlength, $R$, were computed as the expectation value

$$\mu(R) = \mathrm{e}\langle\Psi_M|\sum_i \underline{r}_i|\Psi_N\rangle, \quad (1)$$

where the integral and the summation run over the electron coordinates, denoted by $\underline{r}_i$, and e is the charge of the electron. For permanent dipole moments, the electronic wavefunctions in the bra and ket are the same, i.e. $M = N$, and the dipole moment, which is denoted $\mu(M)$ below, also contains a term due to permanent nuclear charge. For transition dipole moments, $M \neq N$, and the dipole is denoted is $\mu(M - N)$ below. For transition dipole moments, care must be taken to ensure that the dipole phases are consistent as a function of $R$ (Patrascu et al. 2014; Tennyson 2014).

Our calculations produce the values for the dipole at equilibrium given in Table 1 which compare well to the previous results obtained by Zenouda et al. (1999). Our ground state value of the dipole and that of Zenouda et al. (1999) are both slightly smaller than the value 4.60 D used in the JPL data base (Pickett et al. 1998) which was taken from the earlier calculations of Lengsfield & Liu (1982).

Figs 1 and 2 compare our calculated diagonal and off-diagonal DMCs, respectively, with those of Zenouda et al. (1999). The agreement is good. Our calculations suggest that the $\mu(B - A)$ DMC is small at all geometries meaning that the $B - A$ band will be very weak; a similar conclusion was reached by Partridge et al. (1983).

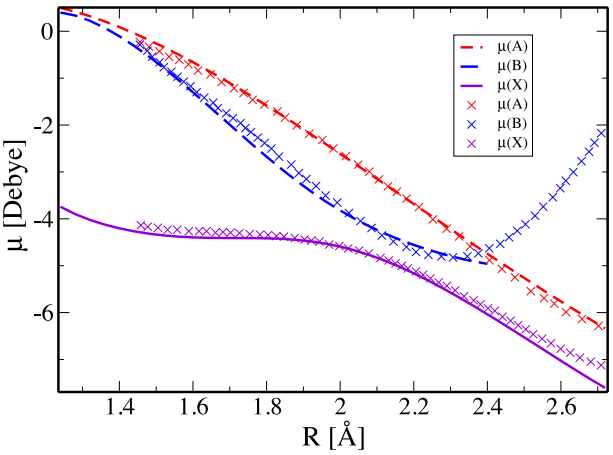


**Figure 1.** Ab initio permanent DMC for AlO for the lowest three electronic states. The previous calculations by Zenouda et al. (1999) are represented by crosses.

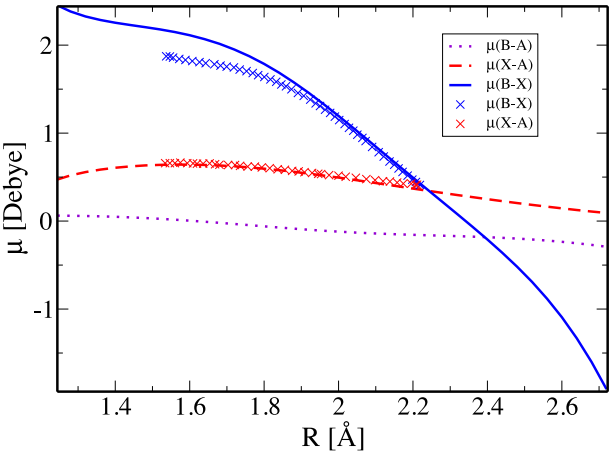


**Figure 2.** Ab initio transition DMC for AlO linking the lowest three electronic states. The previous calculations by Zenouda et al. (1999) are represented by crosses.

The ab initio DMC grid points were used directly in DUO to produce a line list for AlO.

There is a lack of experimental data on AlO transition dipoles or transition intensities. Table 2 therefore compares the lifetime for the $B\,^2\Sigma^+$ state with experimental data available from Johnson, Capelle & Broida (1972), Dagdigian, Cruse & Zare (1975) and two ab initio estimates from Partridge et al. (1983). For Partridge et al. (1983) we have taken their figures which include the small contribution from the weak $B - A$ decay channel since this contribution is also included in our estimate. Our lifetimes were computed by summing over all decays from a given $B\,^2\Sigma^+$ $(v, J)$. Our results in Table 2 are for $J = 0.5$; calculations for $J = 24.5$, which lies in the region of the band head, give lifetimes about 0.5 per cent longer. We conclude that the lifetimes are not strongly $J$-dependent. In common with the other studies we find that the lifetime grows slowly with $v$. Our results are intermediate between the two predictions of Partridge et al. (1983) and slightly shorter than, but marginally consistent with,

**Table 2.** Radiative lifetimes (ns) for $B\,^2\Sigma^+$ state of AlO, compared to the measurements of Johnson et al. (1972) and Dagdigian et al. (1975), and the two separate calculations of Partridge et al. (1983).

| Vibrational level | This work | Partridge et al. (1983) I | Partridge et al. (1983) II | Johnson et al. (1972) | Dagdigian et al. (1975) |
|---|---|---|---|---|---|
| 0 | 92.4 | 88.1 | 109.9 | $128 \pm 6$ | $100 \pm 7$ |
| 1 | 94.5 | 90.5 | 112.6 | $125 \pm 3$ | $102 \pm 7$ |
| 2 | 96.7 | 93.0 | 115.2 | $130 \pm 7$ | $102 \pm 4$ |

**Table 3.** Partition function, $Q(T)$, for $^{27}Al^{16}O$, as a function of temperature.

| $T$ / K | $Q(T)$ | $T$ | $Q(T)$ | Sauval & Tatum (1984) |
|---|---|---|---|---|
| 10 | 134.73 | 1000 | 17 595.69 | 17 693.4 |
| 20 | 265.35 | 2000 | 57 302.56 | 57 060.6 |
| 30 | 396.01 | 3000 | 138 649.47 | 135 168 |
| 40 | 526.68 | 4000 | 283 031.72 | 274 740 |
| 50 | 657.37 | 5000 | 508 066.61 | 487 708 |
| 60 | 788.07 | 6000 | 828 224.93 | 793 980 |
| 70 | 918.78 | 7000 | 1254 881.70 | 1216 536 |
| 80 | 1049.50 | 8000 | 1795 616.84 | 1781 718 |
| 100 | 1310.96 | | | |
| 200 | 2621.45 | | | |
| 300 | 3966.90 | | | |
| 400 | 5407.40 | | | |
| 500 | 6988.27 | | | |
| 600 | 8734.58 | | | |
| 750 | 11 692.87 | | | |

the measurements of Dagdigian et al. (1975). The measurements of Johnson et al. (1972) give longer lifetimes than all studies and we suggest these are too long.

### 2.2 Partition function

Partition functions for AlO were calculated by summing all the calculated energy levels below using DUO (Yurchenko et al. 2015). When summing these levels it is necessary to multiply by the appropriate degeneracy factors. Since we follow HITRAN (Fischer et al. 2003) and use the full nuclear spin degeneracy, the degeneracy factor, $g$, is given by $(2J + 1)(2I_{\rm Al} + 1)(2I_{\rm O} + 1)$, where $J$ is the total angular momentum quantum number obtained by adding the rotational and spin angular momenta. $I_{\rm Al}$ and $I_{\rm O}$ are the nuclear spins of the isotopes of Al and O in the given isotopologue. Explicit inclusion of these nuclear spin factors accounts for hyperfine effects which we make no attempt to resolve. These factors are 11, 6, 1, 6 and 1 for $^{26}$Al, $^{27}$Al, $^{16}$O, $^{17}$O and $^{18}$O, respectively.

Table 3 compares our results for $^{27}Al^{16}O$ with those of Sauval & Tatum (1984). We have multiplied the results of Sauval & Tatum (1984) by the appropriate nuclear spin factors to bring their results into line with our convention outlined above. Table 3 shows good agreement between our $^{27}Al^{16}O$ partition function and that given by Sauval & Tatum (1984) at temperatures above 1000 K for which their results are valid. At lower temperatures we also agree well with the partition function given by JPL (Pickett et al. 1998) who, for example, give $Q(300) = 3926.45$ which is slightly lower than our value of 3966.90, probably due to neglect of the contribution of excited vibrational states.

As we use all ro-vibrational energy levels there are no issues with convergence of this sum. We follow Vidler & Tennyson (2000) and represent our partition function using the following functional form

$$\log_{10} Q(T) = \sum_{n=0}^{8} a_n [\log_{10} T]^n, \qquad (2)$$

where the fitting parameters $a_n$ are given in Table 4. These fits reproduce the partition functions for the entire region below 9000 K with a relative root-mean-square (rms) errors of better than 1.6 per cent.

**Table 5.** Summary of our AlO linelists.

| | $^{27}Al^{16}O$ | $^{27}Al^{18}O$ | $^{26}Al^{16}O$ | $^{27}Al^{17}O$ |
|---|---|---|---|---|
| $X\,^2\Sigma^+$ | | | | |
| Maximum $v$ | 66 | 69 | 66 | 68 |
| Maximum $J$ | 300.5 | 300.5 | 300.5 | 300.5 |
| $A\,^2\Pi$ | | | | |
| Maximum $v$ | 63 | 65 | 62 | 64 |
| Maximum $J$ | 300.5 | 300.5 | 300.5 | 300.5 |
| $B\,^2\Sigma^+$ | | | | |
| Maximum $v$ | 40 | 41 | 39 | 40 |
| Maximum $J$ | 232.5 | 241.5 | 230.5 | 237.5 |
| Number of lines | 4945 580 | 5365 592 | 4866 540 | 5148 996 |

### 2.3 Line list calculations

Line lists were calculated for the four isotopologues $^{27}Al^{16}O$, $^{27}Al^{18}O$, $^{27}Al^{17}O$, and $^{26}Al^{16}O$. All rotation–vibration states were considered and transitions satisfying the dipole selection rule

**Table 4.** Partition function parameters for various isotopologues, see equation (2).

| | $^{27}Al^{16}O$ | $^{27}Al^{18}O$ | $^{26}Al^{16}O$ | $^{27}Al^{17}O$ |
|---|---|---|---|---|
| $a_0$ | −1.040 936 810 38 | −1.597 271 843 92 | −0.677 569 296 333 | −0.541 673 874 468 |
| $a_1$ | 9.640 806 705 54 | 11.984 864 4854 | 9.219 096 681 36 | 10.815 729 0731 |
| $a_2$ | −14.351 233 7912 | −18.294 547 1026 | −13.645 774 0234 | −16.323 002 1925 |
| $a_3$ | 13.062 796 0677 | 16.705 508 6746 | 12.415 493 0773 | 14.878 958 0623 |
| $a_4$ | −7.201 038 286 55 | −9.218 141 947 34 | −6.845 592 401 32 | −8.203 067 510 46 |
| $a_5$ | 2.494 316 830 28 | 3.179 023 188 89 | 2.374 929 555 21 | 2.832 895 713 69 |
| $a_6$ | −0.538 890 191 754 | −0.677 958 762 340 | −0.514 966 111 414 | −0.607 255 974 396 |
| $a_7$ | 0.067 356 850 8718 | 0.082 818 331 0157 | 0.064 742 423 3238 | 0.074 900 937 3167 |
| $a_8$ | −0.003 729 060 501 26 | −0.004 450 320 873 | −0.003 609 777 810 61 | −0.004 077 612 913 49 |

**Table 6.** Extract from the state file for $^{27}Al^{16}O$. Full tables are available from http://cdsarc.u-strasbg.fr/cgi-bin/VizieR?-source=J/MNRAS/.

| $n$ | $\tilde{E}$ | $g$ | $J$ | $+/-$ | $e/f$ | State | $v$ | $\|\Lambda\|$ | $\|\Sigma\|$ | $\|\Omega\|$ |
|---|---|---|---|---|---|---|---|---|---|---|
| 1 | 0.000 000 | 12 | 0.5 | + | e | X2SIGMA+ | 0 | 0 | 0.5 | 0.5 |
| 2 | 965.435 497 | 12 | 0.5 | + | e | X2SIGMA+ | 1 | 0 | 0.5 | 0.5 |
| 3 | 1916.845 371 | 12 | 0.5 | + | e | X2SIGMA+ | 2 | 0 | 0.5 | 0.5 |
| 4 | 2854.206 196 | 12 | 0.5 | + | e | X2SIGMA+ | 3 | 0 | 0.5 | 0.5 |
| 5 | 3777.503 929 | 12 | 0.5 | + | e | X2SIGMA+ | 4 | 0 | 0.5 | 0.5 |
| 6 | 4686.660 386 | 12 | 0.5 | + | e | X2SIGMA+ | 5 | 0 | 0.5 | 0.5 |
| 7 | 5346.116 382 | 12 | 0.5 | + | e | A2PI | 0 | 1 | 0.5 | 0.5 |
| 8 | 5581.906 844 | 12 | 0.5 | + | e | X2SIGMA+ | 6 | 0 | 0.5 | 0.5 |
| 9 | 6066.934 830 | 12 | 0.5 | + | e | A2PI | 1 | 1 | 0.5 | 0.5 |
| 10 | 6463.039 443 | 12 | 0.5 | + | e | X2SIGMA+ | 7 | 0 | 0.5 | 0.5 |
| 11 | 6778.997 803 | 12 | 0.5 | + | e | A2PI | 2 | 1 | 0.5 | 0.5 |
| 12 | 7329.427 637 | 12 | 0.5 | + | e | X2SIGMA+ | 8 | 0 | 0.5 | 0.5 |
| 13 | 7483.145 675 | 12 | 0.5 | + | e | A2PI | 3 | 1 | 0.5 | 0.5 |
| 14 | 8159.170 405 | 12 | 0.5 | + | e | A2PI | 4 | 1 | 0.5 | 0.5 |
| 15 | 8201.467 744 | 12 | 0.5 | + | e | X2SIGMA+ | 9 | 0 | 0.5 | 0.5 |
| 16 | 8857.266 385 | 12 | 0.5 | + | e | A2PI | 5 | 1 | 0.5 | 0.5 |
| 17 | 9029.150 380 | 12 | 0.5 | + | e | X2SIGMA+ | 10 | 0 | 0.5 | 0.5 |
| 18 | 9535.195 842 | 12 | 0.5 | + | e | A2PI | 6 | 1 | 0.5 | 0.5 |
| 19 | 9854.882 567 | 12 | 0.5 | + | e | X2SIGMA+ | 11 | 0 | 0.5 | 0.5 |
| 20 | 10 204.019 475 | 12 | 0.5 | + | e | A2PI | 7 | 1 | 0.5 | 0.5 |
| 21 | 10 667.668 381 | 12 | 0.5 | + | e | X2SIGMA+ | 12 | 0 | 0.5 | 0.5 |
| 22 | 10 864.560 220 | 12 | 0.5 | + | e | A2PI | 8 | 1 | 0.5 | 0.5 |
| 23 | 11 464.897 083 | 12 | 0.5 | + | e | X2SIGMA+ | 13 | 0 | 0.5 | 0.5 |
| 24 | 11 519.212 123 | 12 | 0.5 | + | e | A2PI | 9 | 1 | 0.5 | 0.5 |
| 25 | 12 156.974 798 | 12 | 0.5 | + | e | A2PI | 10 | 1 | 0.5 | 0.5 |
| 26 | 12 257.694 655 | 12 | 0.5 | + | e | X2SIGMA+ | 14 | 0 | 0.5 | 0.5 |
| 27 | 12 793.671 660 | 12 | 0.5 | + | e | A2PI | 11 | 1 | 0.5 | 0.5 |
| 28 | 13 030.412 255 | 12 | 0.5 | + | e | X2SIGMA+ | 15 | 0 | 0.5 | 0.5 |
| 29 | 13 421.583 651 | 12 | 0.5 | + | e | A2PI | 12 | 1 | 0.5 | 0.5 |
| 30 | 13 790.933 964 | 12 | 0.5 | + | e | X2SIGMA+ | 16 | 0 | 0.5 | 0.5 |

*Notes*.
$n$: state counting number.
$\tilde{E}$: state energy in $cm^{-1}$.
$g$: state degeneracy.
$J$: total angular momentum quantum number.
$+/-$: total parity.
$e/f$: rotationless-parity (Brown et al. 1975). State: Electronic term value.
$v$: state vibrational quantum number.
$|\Lambda|$: absolute value of $\Lambda$ (projection of the electronic angular momentum).
$|\Sigma|$: sbsolute value of $\Sigma$ (projection of the electronic spin).
$|\Omega|$: sbsolute value of $\Omega = \Lambda + \Sigma$ (projection of the total angular momentum).

$\Delta J = 0, \pm 1$. These line lists span frequencies up to 35 000 $cm^{-1}$ ($\lambda > 0.286\,\mu m$). The procedure described above was used to produce line lists, i.e. catalogues of transition frequencies $\tilde{\nu}_{ij}$ and *Einstein* coefficients $A_{ij}$, for four Aluminium oxide isotopologues $^{27}Al^{16}O$, $^{27}Al^{18}O$, $^{27}Al^{17}O$ and $^{26}Al^{16}O$. The full line list for each of the studied isotopologues are summarized in Table 5.

## 3 RESULTS

The line lists contain about 5 million transitions each and, therefore, for compactness and ease of use, are divided into separate energy level and transitions file. This is done using standard ExoMol format (Tennyson, Hill & Yurchenko 2013) which is based on a method originally developed for the BT2 line list (Barber et al. 2006). Extracts for the start of the $^{26}Al^{16}O$ files are given in Tables 6 and 7. The full line list for each of these isotopologues can be downloaded from the CDS, via ftp://cdsarc.u-strasbg.fr/pub/cats/J/MNRAS/, or http://cdsarc.u-strasbg.fr/viz-bin/qcat?J/MNRAS/. The partition function and dipole moment data are given as supplementary data to this article. All these plus the potential parameters, as well as the absorption spectrum given in cross-section format (Hill, Yurchenko & Tennyson 2013), can all be obtained from there as well as at www.exomol.com.

Fig. 3 shows the rotational component, and the P- and weaker R-branches of the vibrational fundamental ($v = 0$–1) obtained at $T$= 298 K. As has been noted before (Lengsfield & Liu 1982), the $X$-state dipole is very flat in the equilibrium region. As the strength of a $\Delta v = 1$ vibration–rotation transition depends on the slope of the dipole in this region, this causes the vibrational fundamental to be particularly weak. Therefore this feature, which lies between 10 and 11 μm, is unlikely to be astronomically important. Our calculations suggest that the overtones ($\Delta v > 1$) are also weak so the entire AlO vibration–rotation spectrum is unlikely to feature strongly in astronomical objects.

Much more significant at infrared wavelengths is the $A - X$ electronic band. Fig. 4 shows an overview of the $A - X$ and

**Table 7.** Extracts from the transitions file for $^{27}Al^{16}O$. Full tables are available from http://cdsarc.u-strasbg.fr/cgi-bin/VizieR?-source=J/MNRAS/.

| $f$ | $i$ | $A_{fi}$ |
|---|---|---|
| 47 156 | 47 355 | 1.1598E−04 |
| 9373 | 8773 | 5.0797E−02 |
| 10 989 | 10 389 | 1.5734E−02 |
| 10 789 | 10 589 | 1.5455E−02 |
| 9755 | 9155 | 6.3206E−03 |
| 12 788 | 13 387 | 2.7204E−06 |
| 10 178 | 9578 | 2.3282E−02 |
| 9555 | 9355 | 6.7365E−03 |
| 9187 | 8987 | 5.4996E−02 |
| 9587 | 9387 | 5.4633E−02 |
| 7360 | 7159 | 9.1545E−06 |
| 9184 | 9384 | 4.8954E−05 |
| 9751 | 9151 | 5.9125E−03 |
| 9551 | 9351 | 5.9229E−03 |
| 10 166 | 9566 | 8.9220E−03 |
| 10 985 | 10 385 | 1.4584E−02 |
| 10 785 | 10 585 | 1.4584E−02 |
| 8548 | 7948 | 5.1842E−02 |
| 20 975 | 20 775 | 5.7037E−05 |
| 8148 | 7548 | 5.2229E−02 |
| 9966 | 9766 | 9.1712E−03 |

*Notes*. $f$: upper state counting number; $i$: lower state counting number; $A_{fi}$: Einstein $A$ coefficient in $s^{-1}$.

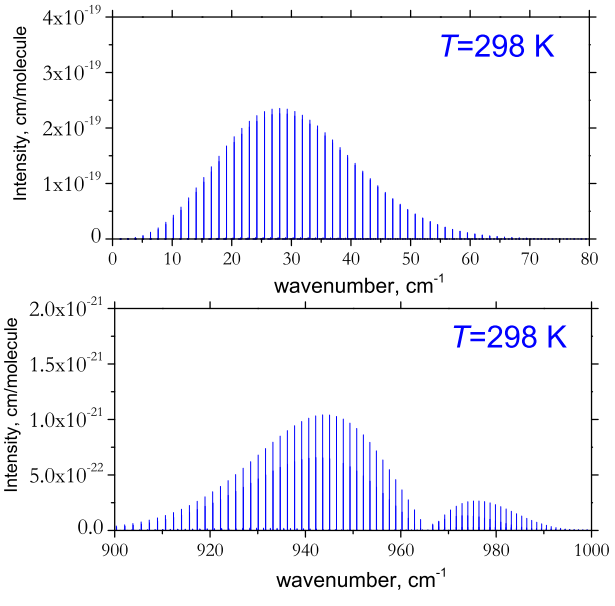


**Figure 3.** Computed spectra of $^{27}Al^{16}O$ at $T$= 298 K given as sticks with the intensity (cm molecule$^{-1}$) represented by their height. Upper panel: rotational region; lower panel: vibrational fundamental.

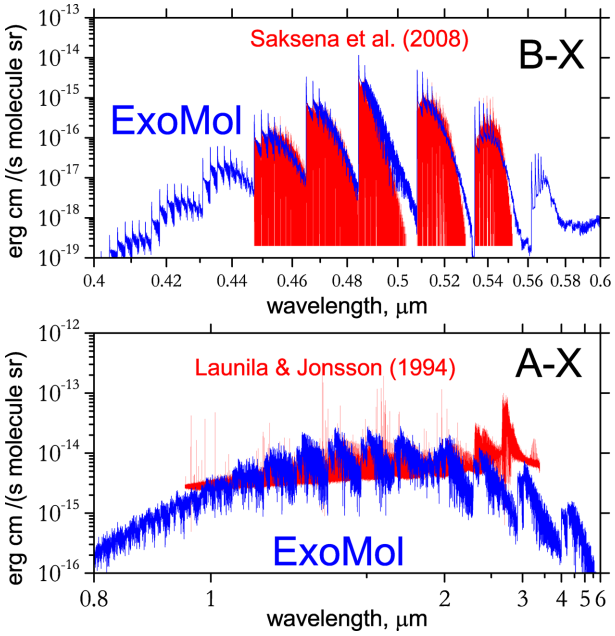


**Figure 4.** Overview of the theoretical (ExoMol) and experimental (Launila & Jonsson 1994; Saksena et al. 2008) spectra of $^{27}Al^{16}O$. The theoretical spectra were obtained as cross-sections convolved with a Gaussian line profile of width 1 cm$^{-1}$ assuming the local thermal equilibrium at $T = 2000$ K. The experimental $A - X$ and $B - X$ spectra are scaled by $1\times 10^{-17}$ and $5\times 10^{-18}$, respectively.

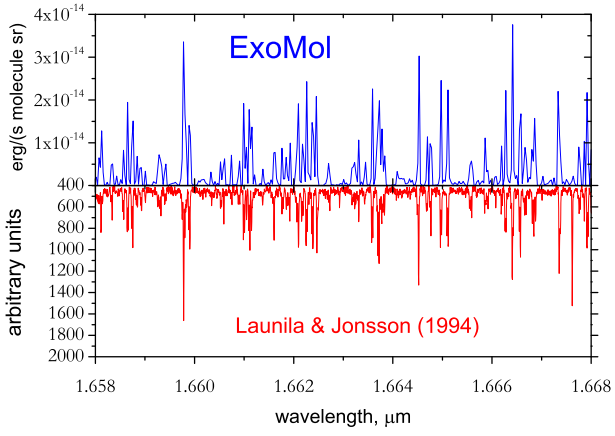


**Figure 5.** A – X emission spectrum of $^{27}Al\ ^{16}O$, comparison with experiments of Launila & Jonsson (1994) at $T$= 3200 K. The theoretical spectrum was obtained as cross-sections convolved with a Doppler line profile assuming the local thermal equilibrium at $T = 3200$ K.

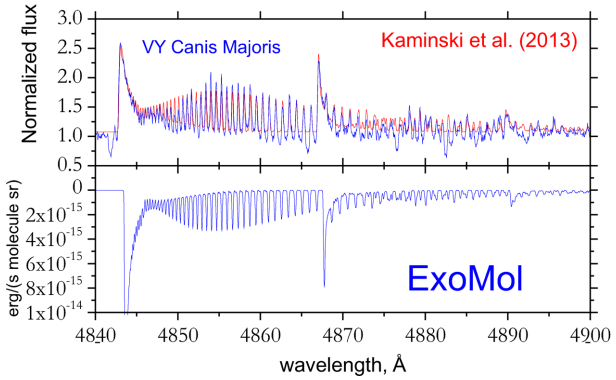


**Figure 6.** $B - X\ \Delta v = 0$ emission spectrum at $T_{\rm rot}$= 700 K and $T_{\rm vib}$= 2200 K compared with an astronomical spectrum obtained by Kaminski et al. (2013) for VY Canis Majoris ($T_{\rm rot}$ and $T_{\rm vib}$ in Kaminski et al. 2013). Cross-sections (lower part) were obtained by convolving with a Gaussian profile of width 0.3 cm$^{-1}$.

$B - X$ electronic transitions which are presented as absorption spectra generated at $T = 2000$ K. Our spectra are compared to available experimental data (Launila & Jonsson 1994; Saksena et al. 2008): we note that these measurements do not give absolute intensities, so have been scaled by us. A more detailed comparison of a portion of the $A - X$ spectrum with the experimental results of Launila & Berg (2011) is presented in Fig. 5. Fig. 6 compares the theoretical spectrum obtained here with an astronomical spectrum of Kaminski et al. (2013). The agreement is remarkable. The calculation performed using the vibrational $T_{\rm vib}$ and rotational $T_{\rm rot}$ temperatures of 2200 and 700 K, respectively, as suggested by Kaminski et al. (2013). We use a Gaussian convolution with the half-width at half-maximum derived of 0.3 cm$^{-1}$ to match the spectrum by Kaminski et al. (2013). Also shown (in red) is the simulation of their observed spectrum by Kaminski et al. (2013); for this they generated their own line list based on the line positions of Saksena et al. (2008), transition moments of Zenouda et al. (1999), Franck-Condon factors of Coxon & Naxakis (1985) and rotational line-strength factors which they computed themselves. We note that our line list provides all these data within a single framework and without making any underlying assumptions about the Franck–Condon approximation or rotational form factors.

Fig. 7 compares the $B - X$ emission spectrum obtained in this work with accurate experimental results of Saksena et al. (2008). Again the agreement is very good. Finally, Fig. 8 compares our calculated spectra $B - X$ for the two isotopologues $^{26}$Al $^{16}$O and $^{27}$Al $^{16}$O. The shift in the band-head feature should be observable astronomically at even moderate resolution.

## 4 CONCLUSIONS

We present comprehensive line lists for the four most important isotopologues of AlO. These are based on the direct solution of the nuclear motion Schrödinger equation using potential energy curves and couplings obtained by fitting to an extensive data set of measured transitions. These data are reproduced to near experimental accuracy resulting in high-accuracy line positions. A new ab initio dipole moment is computed. This dipole is used to compute Einstein $A$ coefficients for all possible dipole-allowed transitions within each AlO isotopologue. The result is a comprehensive line list for each species. The line lists can be downloaded from the CDS, via ftp://cdsarc.u-strasbg.fr/pub/cats/J/MNRAS/, or http://cdsarc.u-strasbg.fr/viz-bin/qcat?J/MNRAS/, or from www.exomol.com.

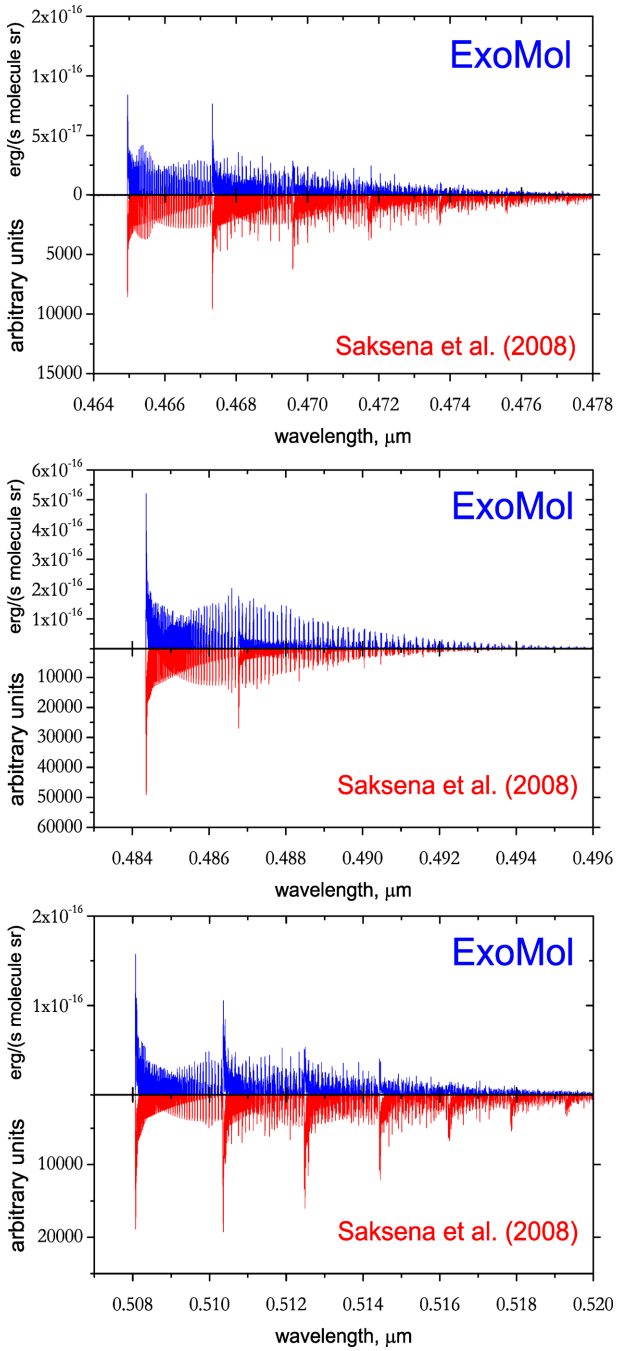


**Figure 7.** Emission spectra of three sub-bands within the $X - B$ band at 1700 K compared to the experiment of Saksena et al. (2008) (up). Top hand panel: $\Delta v = 1$, middle panel: $\Delta v = 0$, lower panel: $\Delta v = -1$. The experimental data is in arbitrary units; calculated cross-sections were obtained by convolving with a Doppler profile at 1700 K.

## ACKNOWLEDGEMENTS

This work is supported by ERC Advanced Investigator Project 267219.

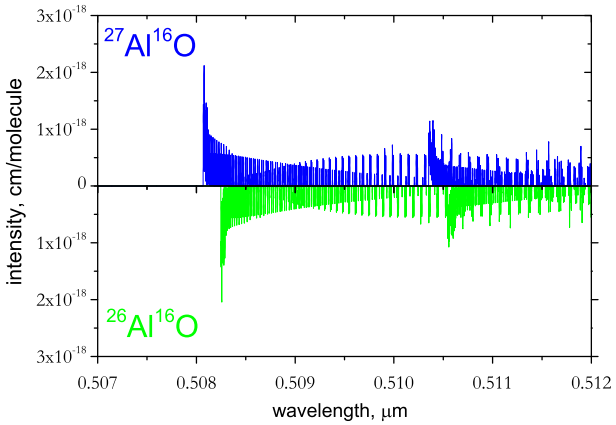


**Figure 8.** Calculated $B - X\ v' - v'' = 0$–1 absorption spectrum at 1700 K for $^{26}Al^{16}O$ and $^{27}Al^{16}O$ obtained by convolving with a Doppler profile at 1700 K.

## REFERENCES


Bai X., Motto-Ros V., Lei W., Zheng L., Yu J., 2014, Spectrochim. Acta B, 99, 193

Banerjee D. P. K., Ashok N. M., Launila O., Davis C. J., Varricatt W. P., 2004, ApJ, 610, L29

Banerjee D. P. K., Barber R. J., Ashok N. K., Tennyson J., 2005, ApJ, 627, L141

Banerjee D. P. K., Varricatt W. P., Mathew B., Launila O., Ashok N. M., 2012, ApJ, 753, L20

Barber R. J., Tennyson J., Harris G. J., Tolchenov R. N., 2006, MNRAS, 368, 1087

Barton E. J., Yurchenko S. N., Tennyson J., 2013, MNRAS, 434, 1469

Barton E. J., Chiu C., Golpayegani S., Yurchenko S. N., Tennyson J., Frohman D. J., Bernath P. F., 2014, MNRAS, 442, 1821

Bernard A., Gravina R., 1984, Z. Nat.forsch. A, 39, 1049

Bescos B., Morley G., Urena A. G., 1995, Chem. Phys. Lett., 244, 407

Brown J. M. et al., 1975, J. Mol. Spectrosc., 55, 500

Coxon J. A., Naxakis S., 1985, J. Mol. Spectrosc., 111, 102

Dagdigian P. J., Cruse H. W., Zare R. N., 1975, J. Chem. Phys., 62, 1824

Fischer J., Gamache R. R., Goldman A., Rothman L. S., Perrin A., 2003, J. Quant. Spectrosc. Radiat. Transfer, 82, 401

Glumac N. G., Servaites J., Krier H., 2001, Combust. Sci. Technol., 172, 97

Hill C., Yurchenko S. N., Tennyson J., 2013, Icarus, 226, 1673

Johnson E. R., 1965, J. Geophys. Res., 70, 1275

Johnson S. E., Capelle G., Broida H. P., 1972, J. Chem. Phys., 56, 663

Kaminski T., Schmidt M. R., Menten K. M., 2013, A&A, 549, A6

Knecht D. J., Pike C. P., Murad E., Rall D. L. A., 1996, J. Spacecr. Rockets, 33, 677

Launila O., Berg L.-E., 2011, J. Mol. Spectrosc., 265, 10

Launila O., Jonsson J., 1994, J. Mol. Spectrosc., 168, 1

Lengsfield B. H., Liu B., 1982, J. Chem. Phys., 77, 6083

Merrill P. W., Keenan P. C., Deutsch A. J., 1962, ApJ, 136, 21

Naulin C., Costes M., 1999, Chem. Phys. Lett., 310, 231

Parigger C. G., Hornkohl J. O., 2011, Spectrochim. Acta A, 81, 404

Partridge H., Langhoff S. R., Lengsfield B. H., Liu B., 1983, J. Quant. Spectrosc. Radiat. Transfer, 30, 449

Patrascu A. T., Hill C., Tennyson J., Yurchenko S. N., 2014, J. Chem. Phys., 141, 144312

Pickett H. M., Poynter R. L., Cohen E. A., Delitsky M. L., Pearson J. C., Müller H. S. P., 1998, J. Quant. Spectrosc. Radiat. Transfer, 60, 883

Saksena M. D., Deo M. N., Sunanda K., Behere S. H., Londhe C. T., 2008, J. Mol. Spectrosc., 247, 47

Sauval A. J., Tatum J. B., 1984, ApJS, 56, 193

Sriramachandran P., Viswanathan B., Shanmugavel R., 2013, Sol. Phys., 286, 315

Surmick D. M., Parigger C. G., 2014, Appl. Spectrosc., 68, 992

Tenenbaum E. D., Ziurys L. M., 2009, ApJ, 694, L59

Tennyson J., 2014, J. Mol. Spectrosc., 298, 1

Tennyson J., Yurchenko S. N., 2012, MNRAS, 425, 21

Tennyson J., Hill C., Yurchenko S. N., 2013, in Gillaspy J. D., Wiese W. L., Podpaly Y. A., eds, AIP Conf. Proc., Vol. 1545, 8th International Conference on Atomic and Molecular Data and Their Applications ICAMDATA-2012. Am. Inst. Phys., New York, p. 186 (doi: 10.1063/1.4815853)

Tylenda R., Crause L. A., Gorny S. K., Schmidt M. R., 2005, A&A, 439, 651

Vidler M., Tennyson J., 2000, J. Chem. Phys., 113, 9766

Werner H. J., Knowles P. J., Lindh R., Manby F. R., Schütz M., 2010, MOLPRO, A Package of Ab Initio Programs. Available at: http://www.molpro.net/

Yadin B., Vaness T., Conti P., Hill C., Yurchenko S. N., Tennyson J., 2012, MNRAS, 425, 34

Yorke L., Yurchenko S. N., Lodi L., Tennyson J., 2014, MNRAS, 445, 1383

Yurchenko S. N., Lodi L., Tennyson J., Stolyarov A. V., 2015, Comput. Phys. Commun.

Zenouda C., Blottiau P., Chambaud G., Rosmus P., 1999, J. Mol. Struct., 458, 61

Zhang S. D., Li H. Y., 2003, Chem. Res. Chin. Univ., 19, 320


## SUPPORTING INFORMATION

Additional Supporting Information may be found in the online version of this article:

1. A spreadsheet containing the computed values of the dipole moments at a grid of geometries.
2. A table giving the temperature-dependent partition function for each isotopologue (http://mnras.oxfordjournals.org/lookup/suppl/doi:10.1093/mnras/stv507/-/DC1).

Please note: Oxford University Press are not responsible for the content or functionality of any supplementary materials supplied by the authors. Any queries (other than missing material) should be directed to the corresponding author for the paper.

This paper has been typeset from a TEX/LATEX file prepared by the author.